Grain boundary characteristics and texture formation in a medium carbon steel during its austenitic decomposition in a high magnetic field

Y D Zhang, C Esling, J.S. Lecomte, C S He, X Zhao, L Zuo

Grain boundary characteristics and texture formation in a medium carbon steel during its austenitic decomposition in a high magnetic field

Y.D. Zhang [a,b], C. Esling [b,*], J.S. Lecomte [b], C.S. He [a], X. Zhao [a], L. Zuo [a]
[a]Key Laboratory of Electromagnetic Processing of Materials (Ministry of Education), Northeastern University, Shenyang 110004, PR China
[b]LETAM, CNRS-UMR 7078, University of Metz, Ile du Saulcy, 57045 Metz, Moselle, France

Abstract

A 12-T magnetic field has been applied to a medium plain carbon steel during the diffusional decomposition of austenite and the effect of a high magnetic field on the distribution of misorientation angles, grain boundary characteristics and texture formation in the ferrite produced has been investigated. The results show that a high magnetic field can cause a considerable decrease in the frequency of low-angle misorientations and an increase in the occurrence of low Σ coincidence boundaries, in particular the Σ3 of ferrite. This may be attributed to the elevation in the transformation temperature caused by the magnetic field and, therefore, the reduction of the transformation stress. The wider temperature range for grain growth offers longer time to the less mobile Σ boundaries to enlarge their areas. Moreover, the magnetic field can enhance the transverse field-direction fiber (〈0 0 1〉 // TFD). It can be assumed that the effects of the field were caused by the dipolar interaction between the magnetic moments of Fe atoms.

Keywords

EPM-electromagnetic processing of materials, Phase transformation, Misorientation, Coincidence site lattice boundary, Texture

1. Introduction

The application of a high magnetic field to the diffusion-controlled phase transformation from austenite to ferrite and then pearlite in steels has been the object of great attention in the area of electromagnetic processing of metallic materials. As the saturation magnetization of the parent and product phases are different, the application of an external magnetic field can modify the Gibbs free energy of phases and then affect the phase equilibrium and transformation speed. The issue has been addressed so far from the thermodynamic, kinetic and metallurgical points of view. The results have shown that there is considerable influence of the magnetic field. It was observed that the magnetic field applied is likely to raise the austenite/ferrite equilibrium temperature [1], [2], [3], [4], [5], [6], accelerate the proeutectoid transformation [6], [7], [8], [9], enhance the amount of the ferrite produced [4], [6], [10], and cause the ferrite grains to align in the field direction [10], [11], [12], [13]. However, no comprehensive study of the influence of a high magnetic field on the characteristics of grain boundaries and texture formation in the phases produced by the diffusional decomposition of austenite was available so far. Deepening these aspects is most likely to permit a better understanding of the way a magnetic field impacts solid phase transformations. In addition, it

will probably yield basic and valuable information leading to an extension of magnetic field application to exert microstructure and property control on metallic materials.

In that context, a hot-forged medium plain-carbon steel was selected and treated without and with the application of a high magnetic field and its influence on the distribution of misorientation angles, grain boundary character distribution (GBCD) and texture of the resulting ferrite was investigated.

2. Experimental

The material used in this study was a medium plain carbon steel with chemical composition (wt.%) 0.49%C, 0.027%Si, 0.074%Mn, 0.24%Cr, 0.0093%P, 0.0086%S and bal. Fe. Specimens of dimensions 30 × 10 × 2 mm were cut from a hot forged bar of an ingot with their longitudinal direction either parallel or perpendicular to the forging deformation direction. They were first water-quenched after complete austenitization at 860 °C to refine the microstructure. They were then re-austenitized at 870 °C for 10 min and cooled at a rate of 23.5 °C/min without and with a 12-T magnetic field. The magnetic field was applied either parallel or perpendicular to the previous deformation direction (DD) to identify the specific influence of the magnetic field. The specimens were placed in the central (zero magnetic force) region.

The above-mentioned specimens were then cut out in their longitudinal direction for further analysis. The transformed microstructure was observed with a JEOL JSM 6500F scanning electron microscope (SEM) and a Philips CM 200 LaB_6 cathode transmission electron microscope (TEM) and the orientation imaging analysis was carried out with the same field emission gun SEM equipped with HKL's Channel 5 software. The 'beam-controlled' mode was applied with a 0.4 μm step. Three different areas were selected on each sample and, to obtain a reliable statistical representation of the results, the total area analyzed covered no less than 2000 ferrite grains and pearlite colonies. As the Kikuchi patterns from the cementite were of low quality, the cementite was not properly indexed by electron backscattering diffraction. Information from pearlite colonies was provided only by its lamellar ferrite and each of them was identified simply as an independent ferrite grain or a part of a proeutectoid ferrite grain, considering that all the ferrite lamellas showed misorientations lower than 10°. The total indexing rate for each area measured was around 93%, of which less than 1% was indexed as cementite. On this basis, the microstructure, misorientation angle distribution, coincidence site lattice (CSL) boundary occurrence and texture were analyzed.

3. Results

The microstructures of the specimens cooled at 23.5 °C/min without and with a 12-T magnetic field are shown in Fig. 1. In both cases – without and with the field – the microstructures are seen to be composed of homogeneously distributed ferrite (equiaxed) and pearlite (lamellar). The application of a magnetic field has reduced effect on the morphology of the microstructure.

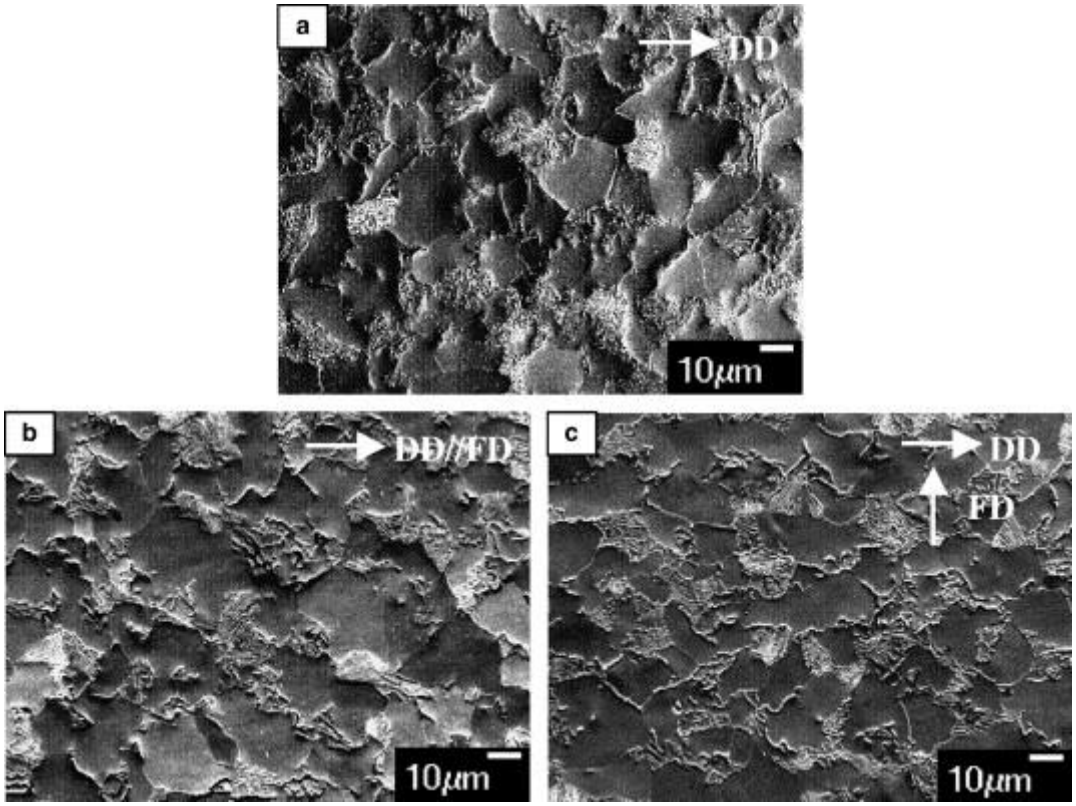

Fig. 1. SEM secondary electron micrographs of specimens austenitized at 870 °C for 10 min and cooled at 23.5 °C/min without and with a 12-T magnetic field. The equiaxed grain areas are proeutectoid ferrite grains and the lamellar areas are pearlite. The deformation direction (DD) is horizontal. (a) 0 T; (b) 12-T field direction (FD)‖DD and (c) 12 T, FD⊥DD.

However, the magnetic field applied shows considerable influence on the substructure of the ferrite produced. The distribution of misorientation angles in ferrite in the specimens submitted or not to a magnetic field is shown in Fig. 2. The misorientation angle distribution in a random cubic polycrystal is also displayed for comparison. It can be seen that, as a whole, low-angle misorientations (2–10°) is considerably less frequent in the specimens treated with the magnetic field. TEM observation shows that there exists in both the non-field-treated and field-treated specimens a large amount of dislocation tangles or pile-ups and networks in both proeutectoid ferrite (Fig. 3(a1) and (b1)) and lamellar ferrite, especially in front of the cementite (Fig. 3(a2) and (b2)). This suggests that the low angle misorientations are caused by these dislocations shown in Fig. 3. Moreover, TEM observation shows that the networks of dislocations in the two kinds of field-treated specimens (FD‖DD and FD⊥DD) are similar to those in the non-field-treated specimens. This indicates that the magnetic field does not impact the dislocation arrangement.

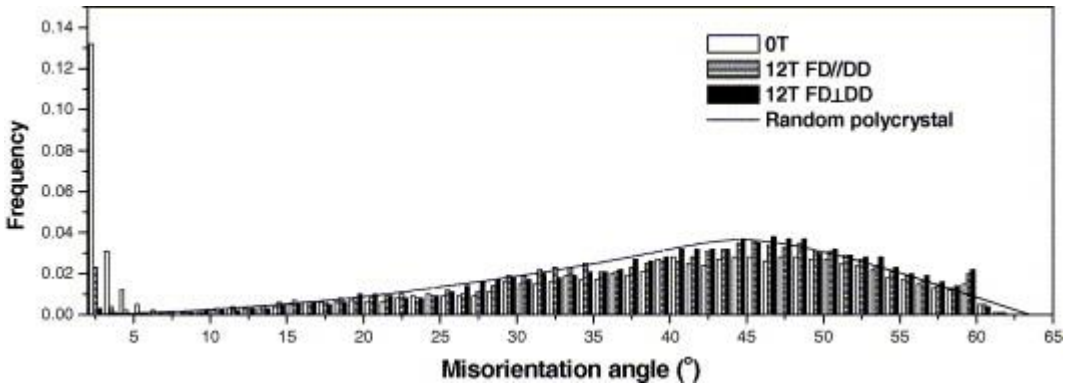

Fig. 2. Misorientation angle distribution of ferrite in specimens austenitized at 870 °C for 10 min and cooled at 23.5 °C/min without and with a 12-T magnetic field.

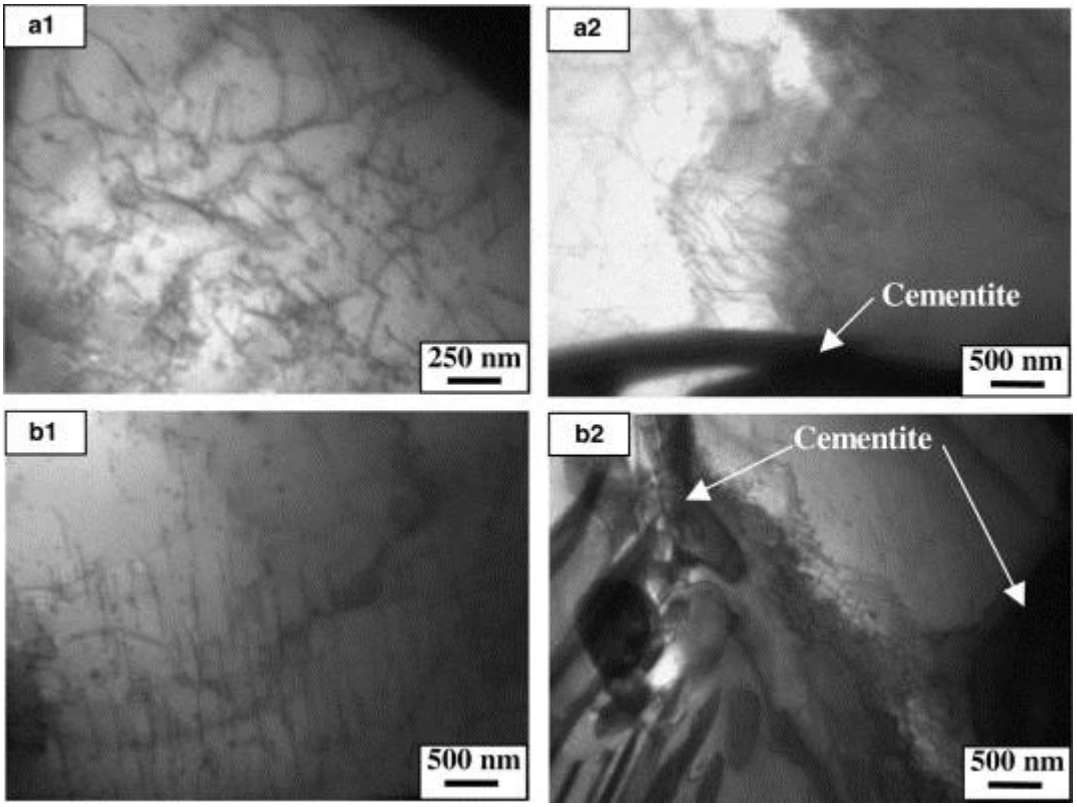

Fig. 3. TEM bright-field micrographs of specimens austenitized at 870 °C for 10 min and cooled at 23.5 °C/min: (a) without and (b) with a 12-T magnetic field (FD‖DD).

Fig. 4 shows the frequency of ferrite CSL boundaries in the specimens cooled without and with the magnetic field. For comparison, the frequency of CSL boundaries in a random polycrystal [14] has also been plotted. It can be seen that, in the presence of the field, the cases of low Σ (Σ3–Σ29) [15] boundaries, especially Σ3 boundaries, are more numerous than those observed without the magnetic field. This result is consistent with the corresponding result obtained with a nanocrystalline nickel sample [15] and a cold-rolled Fe-9 at.%Co alloy annealed under a magnetic field, as shown by Watanabe et al. [16]. The corresponding locations of Σ3 boundaries, for instance, are shown with black lines in Fig. 5. The distribution of boundary length and mean length , computed as an average of 70–100 Σ3 boundaries in each area measured, is shown in Fig. 6 and Table 1. It can be seen in Fig. 5, Fig. 6 and from the data in Table 1 that, when a field is applied, most Σ3 boundaries are longer than those obtained without the magnetic field. This suggests that the higher frequency of Σ boundaries is to be related to their larger boundary areas in field-treated specimens. The results supplied by further analysis on distribution of ferrite grain sizes and mean grain size in the non-field and field-treated specimens are displayed in Fig. 7 and Table 1. It can be seen that the fraction of large grains (>9 μm) (Fig. 7) and the mean grain sizes (Table 1) in the field-treated specimens are higher than that observed in the non-field-treated specimen. This shows that the larger Σ3 boundary areas are related to larger grain sizes in the field-treated specimens and the field applied has some effect on grain growth.

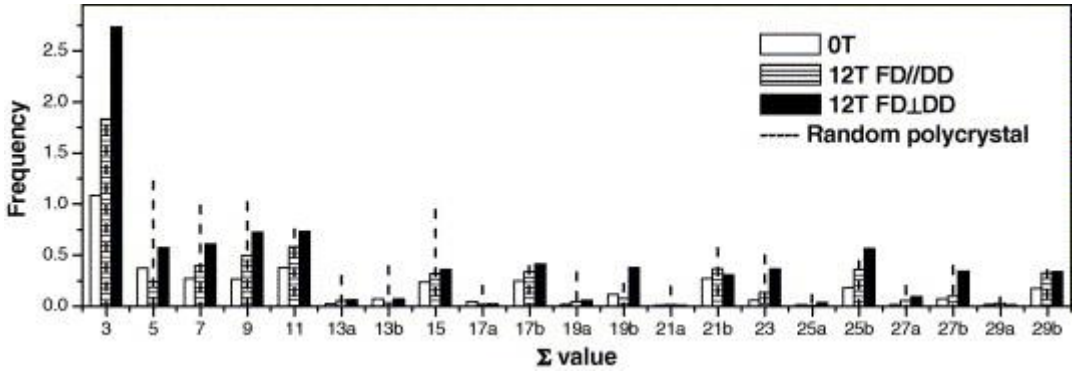

Fig. 4. Frequencies of CSL boundaries in specimens austenitized at 870 °C for 10 min and cooled at 23.5 °C/min without and with a 12-T magnetic field.

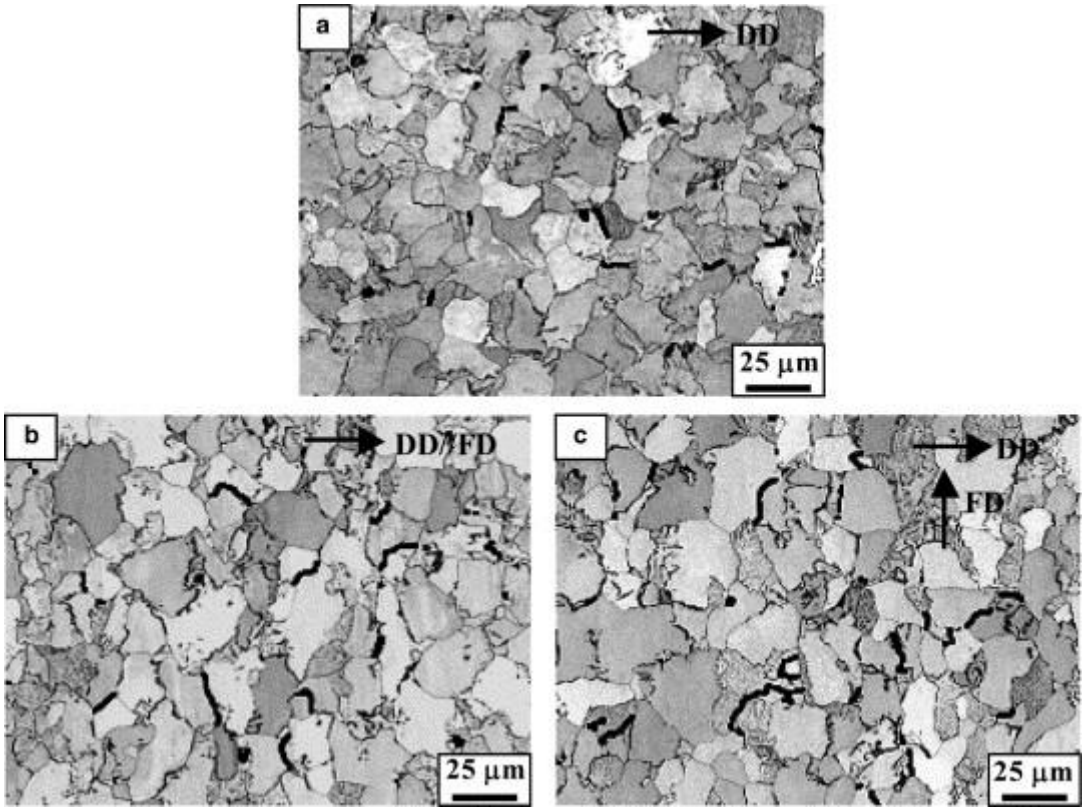

Fig. 5. Orientation maps of specimens austenitized at 870 °C for 10 min and cooled at 23.5 °C/min without and with a 12-T field. The deformation direction (DD) is horizontal. (a) 0 T; (b) 12 T, FD∥DD; (c) 12 T, FD⊥DD. Black lines display the Σ3 boundaries.

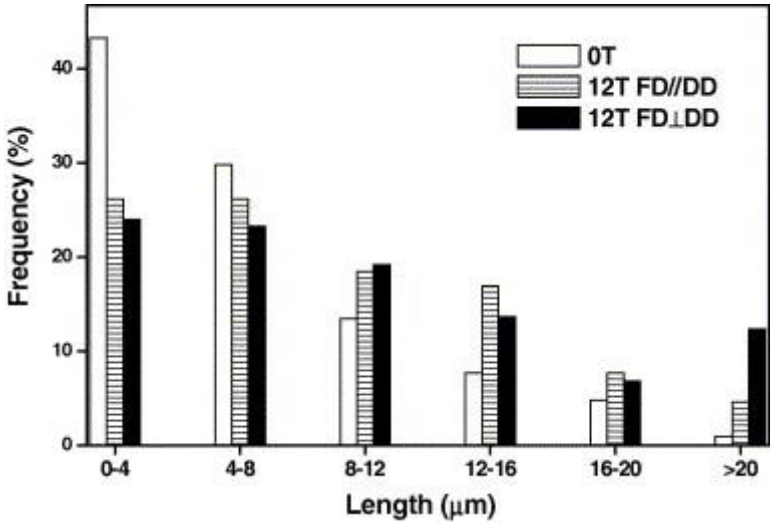

Fig. 6. Length distribution of Σ3 boundaries in specimens austenitized at 870 °C for 10 min and cooled at 23.5 °C/min without and with a 12-T field.

Table 1. Mean length of Σ3 boundaries and mean grain size of ferrite in specimens austenitized at 870 °C for 10 min and cooled at 23.5 °C/min without and with a 12-T field

	0 T	12 T, FD‖DD	12 T, FD⊥DD
$\bar{L}$ (μm)	5.96	8.62	10.20
$\bar{d}$ (μm)	14.05	15.57	15.34

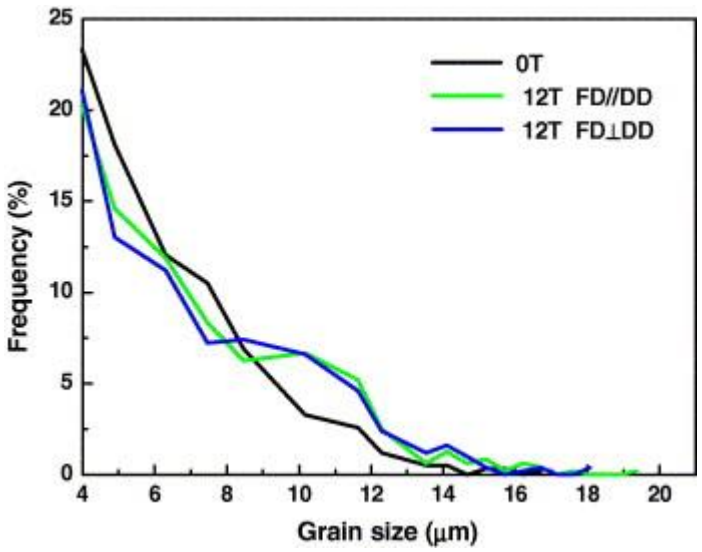

Fig. 7. Grain size distribution of specimens austenitized at 870 °C for 10 min and cooled at 23.5 °C/min without and with a 12-T field.

The inverse pole figures of the specimens treated without and with the magnetic field and the corresponding sample coordinates are shown in Fig. 8. It can be clearly seen that there is an enhancement of the 〈0 0 1〉 fiber texture component along the transverse field direction (TFD) in the two field-treated specimens (FD‖DD and FD⊥DD). This shows that the enhancement of this fiber component is solely due to the presence of the field, and not to prior deformation. The grains with their 〈0 0 1〉 parallel to the TFD (〈0 0 1〉 ‖TFD grains) in the field-treated specimens are identified by using the "texture component" function of Channel 5 and displayed in blue in Fig. 9. As

the magnetic field was applied either along the prior deformation direction (DD) or perpendicular to DD (or ∥TD), TFD has correspondingly two orientations, i.e. parallel to TD or to DD. So, for comparison, in the non-field-treated specimen, the corresponding 〈0 0 1〉 ∥TD or DD grains were identified and displayed in the same figure. A 10° deviation from the exact 〈0 0 1〉 ∥TFD orientation is allowed according to the spreading degree of the 〈0 0 1〉 ∥TFD fiber component in the inverse pole figures in Fig. 8. By comparing Fig. 9(b) with (a) and (d) with (c), it can be seen that, when a field is applied, the 〈0 0 1〉 ∥TFD grains (in blue) cover a larger area than the 〈0 0 1〉 ∥TD or 〈0 0 1〉 ∥DD grains in the non-field-treated specimen. The formation of this fiber component could be the result of either a preferential nucleation or preferential grain growth of 〈0 0 1〉 ∥TFD grains, or both. To clarify this point, the percentage (numberwise) of 〈0 0 1〉 ∥TFD grains in relation to the total grain population, their average size in each field-treated specimen, and the corresponding percentage of 〈0 0 1〉 ∥TD (or DD) in the non-field-treated specimens have been analyzed with Channel 5. The results are given in Table 2. For comparison, the mean grain size of the total population in each specimen is also given (in brackets). It can be seen that, when a field is applied, the percentage of 〈0 0 1〉 ∥TFD grains is higher than that in the non-field-treated specimen. Moreover, in the latter case, the average size of the 〈0 0 1〉 ∥TD or 〈0 0 1〉 ∥DD grains is either close to or slightly smaller than the average computed over all grains, whereas, in the field-treated specimens, the average size of the 〈0 0 1〉 ∥TFD grains is higher than the average value of the whole population. This suggests that the formation of the 〈0 0 1〉 ∥TFD fiber component is related to both preferential nucleation and preferential grain growth.

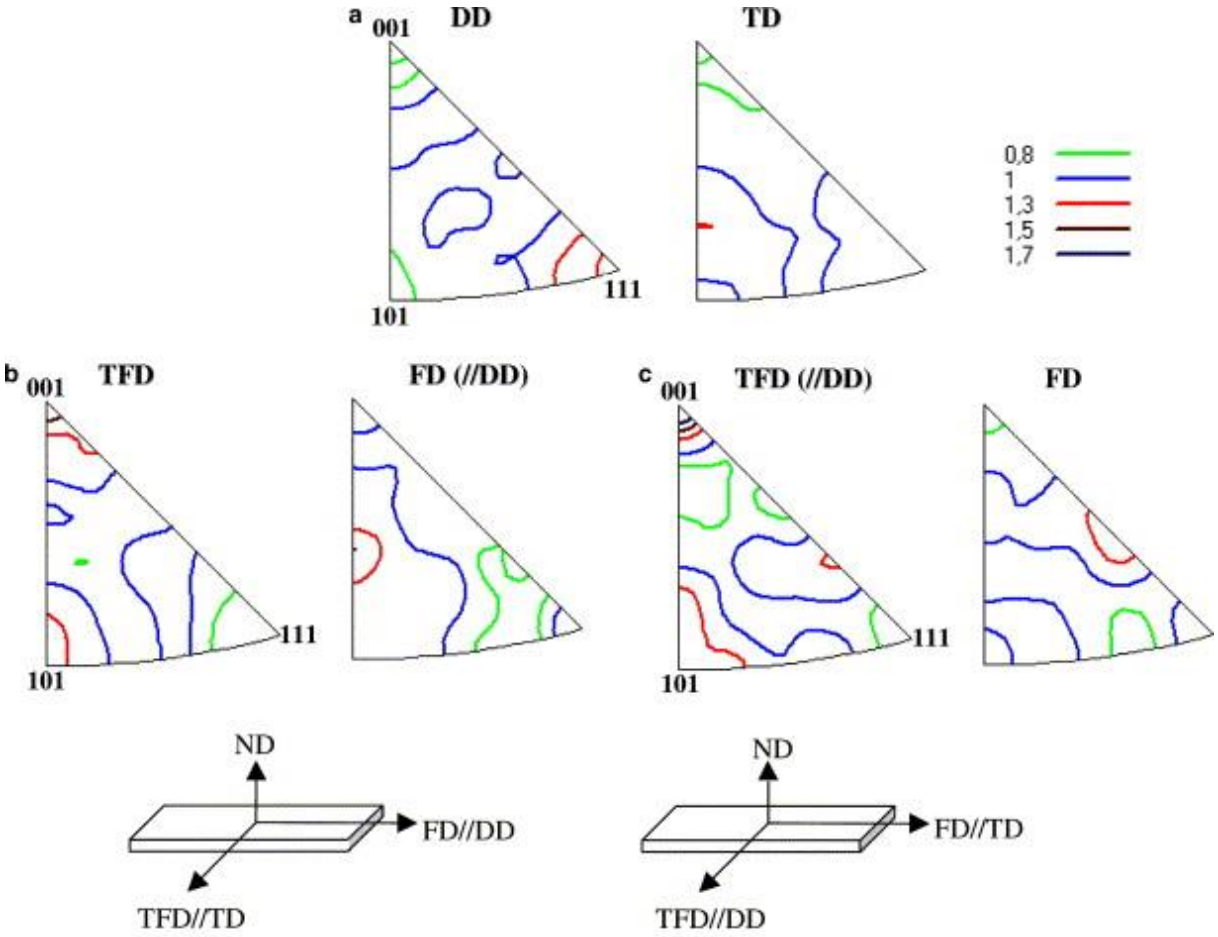

ND: Specimen normal direction
DD: Deformation direction
TD: Transverse deformation direction
FD: Field direction
TFD: Transverse field direction

Fig. 8. Inverse pole figures of specimens treated without and with a 12-T magnetic field and corresponding sample coordinates. (a) 0 T; (b) 12 T, FD∥DD and (c) 12 T, FD⊥DD.

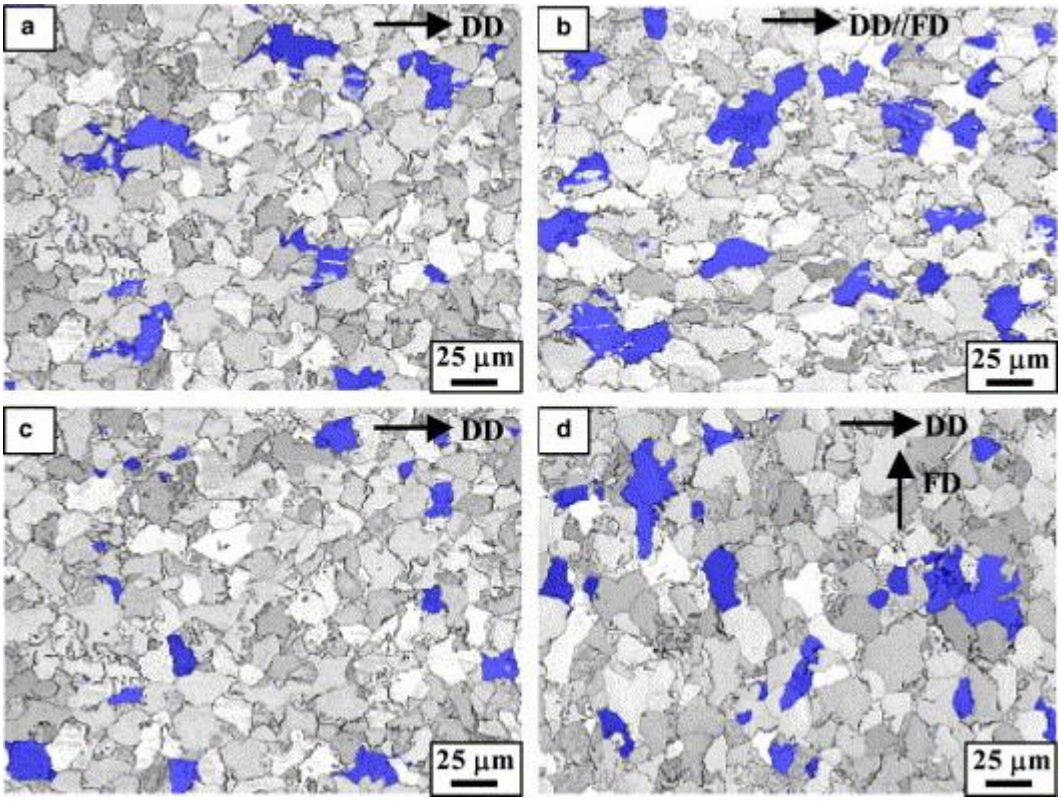

Fig. 9. Orientation micrographs of specimens austenitized at 870 °C for 10 min and cooled at 23.5 °C/min without and with a 12-T magnetic field, showing the crystallographic orientation of ferrite grains by color. The deformation direction is horizontal. (a) 0 T, blue: 〈0 0 1〉 ∥TD; (b) 12 T, FD∥DD, blue: 〈0 0 1〉 ∥TFD (or TD); (c) 0 T, blue: 〈0 0 1〉 ∥DD; (d) 12 T, FD⊥DD, blue: 〈0 0 1〉 ∥TFD (or DD). (For interpretation of the references to colour in this figure legend, the reader is referred to the web version of this article.)

Table 2. Percentage (numberwise) and mean size of grains with their 〈0 0 1〉 parallel to TFD in the field-treated specimens and grains with 〈0 0 1〉 parallel to either TD or DD in the non-field-treated specimen

	12 T, FD∥DD (TFD∥TD)	0 T, (⟨0 0 1⟩∥TD)	12 T, FD⊥DD (TFD∥DD)	0 T, (⟨0 0 1⟩∥DD)
Percentage (numberwise) (%)	7.89	5.00	7.31	5.52
Mean grain size (µm)	17.56 (15.57)	14.04 (14.05)	16.93 (15.34)	13.46 (14.06)

4. Discussion

With fully austenitized medium carbon steels, austenite is transformed first into equiaxed ferrite (called proeutectoid ferrite) between the Ar_3 and Ar_1 temperature, and then into pearlite (consisting of alternately distributed eutectoid ferrite and cementite lamellae) below Ar_1 during the subsequent cooling, as seen in Fig. 1.

Given the same amount of Fe atoms, the volume of bcc ferrite is larger than that of fcc austenite. This generates a transformation stress and thus strain. The transformation stress is temperature-dependent for a given cooling rate. This stress increases with the decreasing temperature for transformation. When the stress accumulates up to a specific threshold, it can be released through the deformation of the softest phases, i.e. ferrite in the case of austenite-to-ferrite and then ferrite-to-pearlite transformation [17]. This stress rises when pearlite is formed as the process involves the development of two phases with different crystal structures and therefore different volume changes. Moreover, the cementite lamellae are embedded in

alternation in the eutectoid ferrite. This transformation strain accounts for the formation of a large amount of dislocations observed in both proeutectoid and, especially, eutectoid ferrite, which results in low angle misorientations, as shown in Fig. 2.

Applying the Johnson–Mehl equation, the volume fraction f of a product phase during solid-state phase transformation is determined by its nucleation rate $\dot{N}$, growth rate v and transformation time t, i.e.,

$$f = 1 - \exp\left(-\frac{A}{4}\dot{N}v^3t^4\right) \quad (1)$$

where A is the shape factor of the nuclei. By taking the features of phase transformation in medium carbon steels into account, the kinetic equation of proeutectoid ferritic transformation from austenite can be expressed as [18]

$$\ln t = B\ln\left(\ln\frac{1}{1-f}\right) + C\frac{Q}{RT} + E\frac{\sigma^3}{\Delta G_V^2} - F\ln\frac{x^\gamma - x}{x^\gamma - x^\alpha}, \quad (2)$$

where B, C, E, R and F are constants, Q is the activation energy for diffusion, T is the absolute temperature, σ is the interfacial energy, ΔG_V is the driving force of the transformation or Gibbs free energy difference between the parent and the product phase, x^γ and x^α are the carbon solubility of austenite and ferrite at T, and x is the carbon content in the initial austenite. When a high magnetic field is applied, both parent austenite and product ferrite can be magnetized to some extent and the corresponding Gibbs free energy is thus lowered [11]. Since the degree of magnetization of ferrite is higher than that of austenite [4], the decrease in the Gibbs free energy is larger for ferrite than for austenite, which results in additional magnetic Gibbs free energy difference between ferrite and austenite or additional driving force ΔG_M. In this case, ΔG_V in Eq. (2) should be replaced by $\Delta G_V + \Delta G_M$. ΔG_M is negative, i.e., has the same sign as ΔG_V and contributes by more than 15% to the sum of $\Delta G_V + \Delta G_M$ [6]. As a consequence, the incubation time for the transformation from austenite to ferrite is reduced. This kinetic characteristic can be easily illustrated with the CCT diagram of the steel, as shown in Fig. 10. By reducing the incubation time, the magnetic field shifts the starting and finishing lines of the transformation to the left (Fig. 10). Consequently, the transformation is shifted towards the higher temperature area. By elevating the transformation temperature, the transformation stress is reduced. As a result, less transformation strain is created and the number of low-angle misorientations is correspondingly decreased by the application of the magnetic field (Fig. 2).

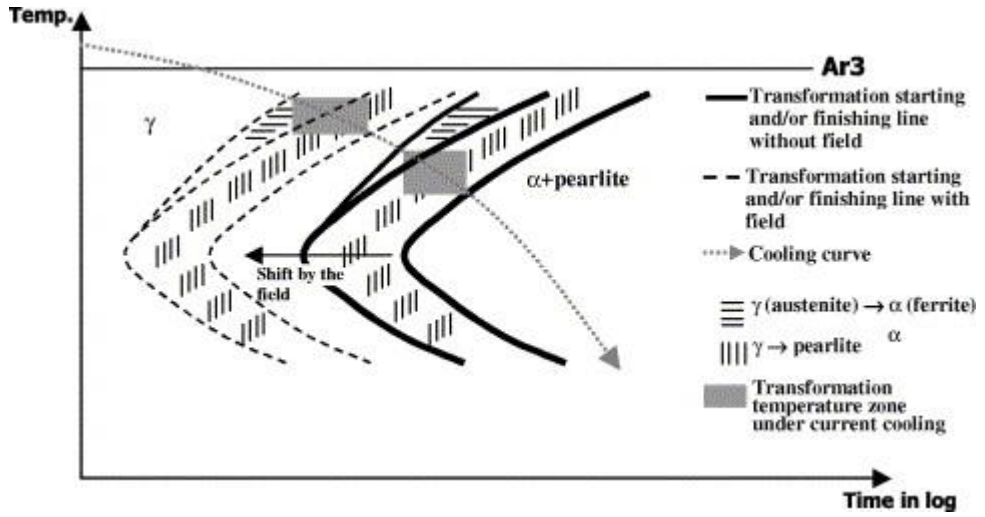

Fig. 10. Schematic illustration of the CCT curves, without and with a magnetic field. The magnetic field has an influence on the transformation by shifting the transformation zone to higher temperature and shorter time ranges

The application of the magnetic field has also a considerable effect on the occurrence of the coincidence site lattice (CSL) boundaries as shown in Fig. 4. It increases the frequency of almost all low Σ boundaries, especially Σ3. It is known that different types of grain boundaries have different energy and mobility. The random high-angle boundaries have high energy and high mobility, whereas some low Σ boundaries – especially the Σ3 boundaries – have low energy and low mobility [19]. For grains with different types of boundaries, the growth through boundary migration will cause the low mobility types to enlarge their boundary areas whereas the high mobility types will shrink [20]. Hence, after growth, the proportion of low mobility boundaries will increase. In the present work, the transformation from austenite to ferrite and pearlite in this material, without applying a field, ends at about 650 °C. Ferrite grains continue to grow after the transformation. Therefore, the proportion of the various types of ferrite grain boundaries start changing. As the magnetic field can raise the transformation temperature, both proeutectoid and eutectoid ferrite in the field-treated specimens grow within a wider temperature range. As a result, the proportion of low mobility Σ boundaries, especially Σ3, obtained under the magnetic field is raised. In this case, the higher frequency of Σ boundaries shown in Fig. 4 under the magnetic field is the result of excessive grain growth.

The applied magnetic field also clearly enhances the ⟨0 0 1⟩ fiber texture component along the TFD, and this appears in both cases FD∥DD and FD⊥DD, as seen in Fig. 8. This result is quite different from the result found in the cold-rolled steels annealed under a magnetic field. In those cases, the enhancement of the ⟨0 0 1⟩ component appeared along the field direction (FD) [16], [21], [22], [23]. According to the analysis in [21], the anisotropic magnetization in different crystallographic directions accounts for the formation of ⟨0 0 1⟩ // FD fiber component. Nuclei with the ⟨0 0 1⟩ directions (easiest magnetization direction) parallel to the field direction have the largest driving force for recrystallization. However, in the present work, the enhancement of the ⟨0 0 1⟩ component appears in the TFD, which suggests that the field acts in a different way. It is well known that each iron atom carries a magnetic moment. Under the magnetic field applied, these moments tend to align along the field direction, as schematically illustrated in Fig. 11(a). Then, there exists a dipolar interaction between neighboring atoms. Let the magnetic moment of each atom be *m* and the distance between two neighboring atoms *r*. The magnetic moments align along the field

direction, as shown in Fig. 11(b). The dipolar interaction energy E_D can then be obtained by rearranging the related equations in [24]

$$E_D = -\frac{\mu_0 m^2}{4\pi}\frac{3\cos^2\theta - 1}{r^3}, \quad (3)$$

where μ_0 is the vacuum magnetic permeability. E_D is ϑ- and r-dependent. The variation of the geometrical factor in Eq. (3) as a function of ϑ for different r values has been calculated and is shown in Fig. 12. It can be seen that, when $\vartheta = 0°$ or 180°, i.e., the pairs of moments aligned are parallel to FD, E_D is minimum (negative); whereas, when $\vartheta = 90°$, i.e., the pairs aligned are parallel to TFD, E_D is maximum (positive). Therefore, the atoms attract each other along the FD, but repel each other along the TFD. Correlatively, the distance between neighboring atoms tends to decrease along FD and increase along TFD. This atomic spacing increase in TFD may mitigate the solution distortion of carbon atoms in some specially orientated grains, thus affecting their nucleation and growth. In ferrite, the carbon atoms are located in the octahedral interstices, as shown in Fig. 13. The interstices are flattened in the 〈0 0 1〉 direction. The occupation of this interstice by the carbon atom submits neighboring iron atoms to an expansion stress along the 〈0 0 1〉 direction. This gives rise to lattice distortion and creates distortion energy. If the 〈0 0 1〉 direction of a grain is parallel to the TFD, the lattice distortion energy is reduced by increasing the atomic spacing in the 〈0 0 1〉 direction due to dipolar repulsion. Consequently, the nucleation and growth of those grains is most energetically favored by the magnetic field, and the 〈0 0 1〉 ∥TFD component is enhanced.

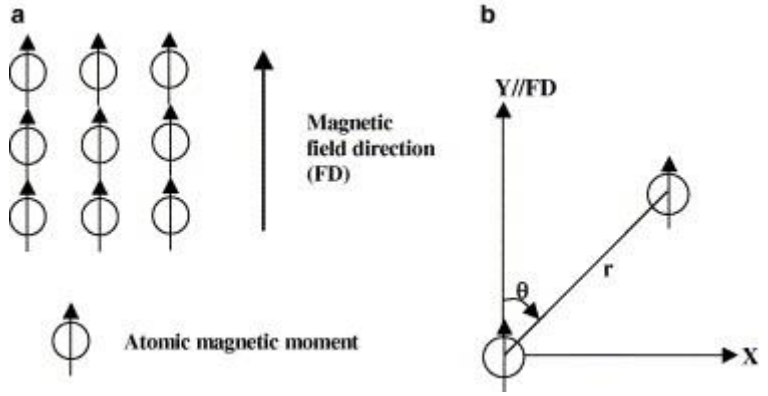

Fig. 11. (a) Schematic illustration of the alignment of atomic magnetic moments under the magnetic field applied; (b) Position between two neighboring atomic moments correlated in a coordinate system.

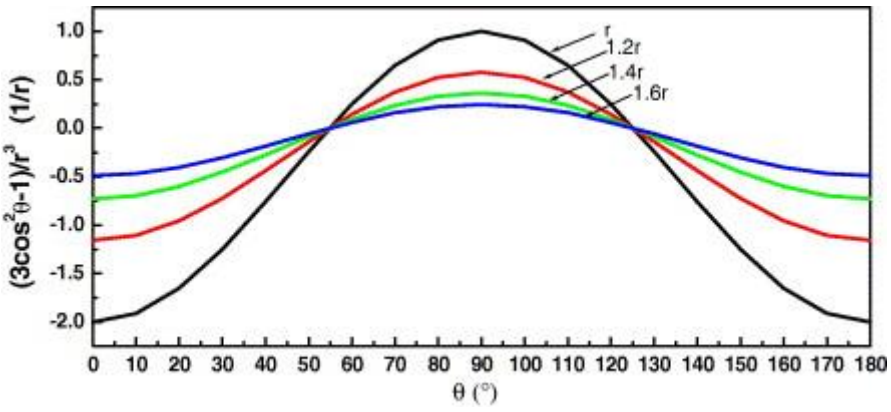

Fig. 12. Variation of the geometrical factor of the dipolar interaction energy E_D as a function of ϑ with different r values.

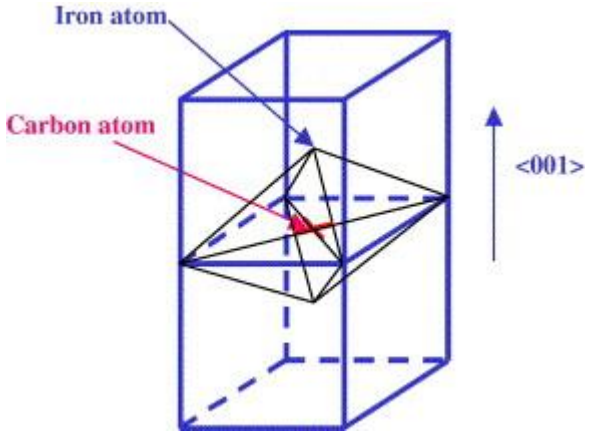

Fig. 13. Location of a carbon atom in an octahedral interstice of the bcc lattice.

5. Conclusions

1.The magnetic field considerably lowers the occurrence of the low angle misorientations in ferrite. This is attributed to the rise of the transformation temperature by the magnetic field and hence the decrease of the transformation stress and thus strain.

2.The magnetic field strongly raises the frequency of Σ3–29 coincidence boundaries in ferrite, especially the Σ3 boundaries. This occurs through selective area enlargement of low-mobility boundaries during the growth stage.

3.The magnetic field enhances the 〈0 0 1〉 texture component along the TFD. This is a result of the preferential nucleation and growth of grains with 〈0 0 1〉 parallel to the TFD, as a consequence of the dipolar interaction of the magnetic moments carried by the iron ferrite atoms.

Acknowledgements

This study was financially supported by the National Science Fund for Distinguished Young Scholars (Grant No. 50325102), the key project of National Natural Science Foundation of China (Grant No. 50234020), and the TRAPOYT in Higher Education Institutions of MOE, PRC.

The authors also gratefully acknowledge the support obtained in the frame of the Chinese–French Cooperative Research Project (PRA MX04-02).

The authors are grateful of Mr. P. Barges (IRSID ARCELOR RESEARCH) for the help of TEM work.

References

[1] A.K. Ghosh, M.N. Roy, Trans Indian Inst Met, 40 (1987), p. 329
[2] H.D. Joo, S.U. Kim, N.S. Shin, Y.M. Koo
Mater Lett, 43 (2000), p. 225
[3] H. Guo, M. Enomoto, Mater Trans JIM, 41 (2000), p. 911
[4] J.-K. Choi, H. Ohtsuka, Y. Xu, W.-Y. Choo, Scripta Mater, 43 (2000), p. 211
[5] C.T. Peters, A.P. Miodownik, Scripta Metall, 7 (1973), p. 955

[6] Y.D. Zhang, C.S. He, X. Zhao, L. Zuo, C. Esling, J.C. He, J Magn Magn Mater, 294 (2005), p. 267
[7] M. Enomoto, H. Guo, Y. Tazuke, Y.R. Abe, M. Shimotomai, Metall Mater Trans, 32A (2001), p. 445
[8] Y.D. Zhang, C.S. He, X. Zhao, C. Esling, L. Zuo, Adv Eng Mater, 6 (2004), p. 310
[9] Y.D. Zhang, C.S. He, X. Zhao, L. Zuo, C. Esling, J.C. He, J Magn Magn Mater, 284 (2004), p. 287
[10] M. Shimotomai, K. Maruta, Scripta Mater, 42 (2000), p. 499
[11] M. Shimotomai, K. Maruta, K. Mine, M. Matsui, Acta Mater, 51 (2003), p. 2921
[12]K. Maruta, M. Shimotomai, J Cryst Growth, 237–239 (2002), p. 1802
[13] H. Ohtsuka, Y. Xu, H. Wada, Mater Trans JIM, 41 (2000), p. 907
[14] L. Zuo, C. Esling, Scripta Metall Mater, 32 (1995), p. 937
[15] K. Harada, S. Tsurekawa, T. Watanabe, G. Palumbo, Scripta Mater, 49 (2003), p. 367
[16] T. Watanabe, Y. Suzuki, S. Tanii, H. Oikawa, Philos Mag Lett, 62 (1990), p. 9,
[17] R. Pandi, S. Yue, ISIJ Int, 34 (1994), p. 270
[18] H.B. Chang, Z.G. Li, T.Y. Hsu, X.Y. Ruan Acta Metall Sinica (English Lett), 11 (1998), p. 207
[19] F.J. Humphreys, M. Hatherlyb **Recrystallization and related annealing phenomena** Pergamon Press, New York (NY) (1995)p. 300
[20] Y.D. Zhang, G. Vincent, N. Dewobroto, L. Germain, X. Zhao, L. Zuo, *et al.*J Mater Sci, 40 (2005), p. 905
[21] H.O. Martikainen, V.K. Lindroos Sc and J Metall, 10 (1981), p. 3
[22] N. Masahashi, M. Matsuo, K. WatanabeJ Mater Res, 13 (1998), p. 457
[23] C.S. He, Y.D. Zhang, X. Zhao, L. Zuo, J.C. He, K. Watanabe, *et al.*Adv Eng Mater, 5 (2003), p. 579
[24] M. Cyrot, *et al.* **Magnétisme** Presses Universitaires de Grenoble, Grenoble (1999)p. 37, 65